Feasibility Analysis of Small-Size Space Debris Removal in Low-Earth Orbit by Space-Based Laser Ablation

Elias Bögel[(1)], Hugo Buurmeijer[(2,3)], Lorenz Veithen[(3)], Frank Meijering[(3)], Gabriel Alves Teixeira[(3)], Daniel Rehling[(3)], Juan Bas Fernández[(3)], Per van Wolfswinkel[(3)], Niek Zandvliet[(3)], Jan Struziński[(3)]

[(1)]Delft Institute of Applied Mathematics, Delft University of Technology
Delft, The Netherlands
Email: ebogel@tudelft.net

[(2)]Aeronautics & Astronautics, Stanford University
Stanford, United States of America
Email: hbuurmei@stanford.edu

[(3)]Faculty of Aerospace Engineering, Delft University of Technology
Delft, The Netherlands
Email: lveithen@ tudelft.net

***Abstract* – As artificial objects in Low Earth Orbit (LEO) become more numerous, the risk for breakup events threatening space-based services increases rapidly. Laser ablation methods have previously been proposed for the removal of small-size (1 - 10 cm) debris fragments, but a mission-level feasibility study is yet to be performed. This work investigates the mission concept and spacecraft design feasibility of a space-based laser aiming to de-orbit 50% of the debris generated by an on-orbit catastrophic event, using an agent-based modelling approach applied to the 2009 Cosmos-Iridium collision example. Several parameters were varied to generate a feasibility envelope on the payload performance, showing that the necessary capabilities for mission feasibility are within ranges achievable with current or near-term technology. A cost estimate for a single-flight mission of 550 M€ was generated based on the conceptual design developed for this study and is in agreement with previous research. This work shows that a laser ablation concept for the removal of small-size debris in LEO is feasible both technically and financially. It further provides a modelling base for future research on similar concepts for different mission scenarios.**

I. INTRODUCTION

Over the past 60 years, mankind has continuously expanded its exploration and utilisation of near-Earth space, growing society's reliance on space systems [1]. However, many spacecrafts do not have a sustainable End of Life (EoL) strategy or are unable to remove themselves from orbit in case of failure, resulting in numerous space debris in near-Earth space. With the ever-growing launch traffic in Low Earth Orbit (LEO) [2], the number of uncontrollable large objects has steadily risen. This increases the likelihood of an exponential growth in space debris population due to the cascading collision effect theorised by Kessler and Cour-Palais in 1978 [3], known as the "Kessler syndrome". The syndrome predicts the denial of protected space regions through space debris build-up and its onset can already be observed in Fig. 1. However, recent trends have intensified the problem as thousands of satellites are launched to form mega-constellations in LEO [4].

Although break-up events most commonly occur resulting from explosions or, more recently, Anti-Satellite (ASAT) weapon tests [5, 6], [3] predicted collisions to become a major source of debris. The steep increase in large man-made (uncontrollable) objects in LEO strongly increases the risks of collisions yielding a breakup event where objects are broken up into several smaller debris. The most dangerous being 1-10 cm large space debris as they can render active satellites inoperable upon collision, while being difficult to track due to their small size. Two historically large breakup events were the Chinese ASAT weapon test targeting the Fengyun-1C satellite in January 2007 and the collision between the Iridium 33 satellite and the defunct Cosmos 2251 satellite. The magnitude of these events was large enough to produce a clear jump in the number of catalogued objects orbiting Earth, visible in Fig. 1.

After a breakup event, the debris cloud is first localised on the initial spacecraft orbit but quickly spreads over the globe as shown in Fig. 2 [7, 8]. First, the distribution in ejection velocities results in different orbital periods in the debris population, meaning that the cloud spreads over the original orbit. Second, small variations in debris orbital elements result in a different evolution of the Right Ascension of the Ascending Node (RAAN) because of the J2-effect, ultimately separating the fragment orbits and covering the full globe [9]. Therefore, cleaning-up of small space debris is most efficient right after the collision, when most debris objects are in very similar orbits.

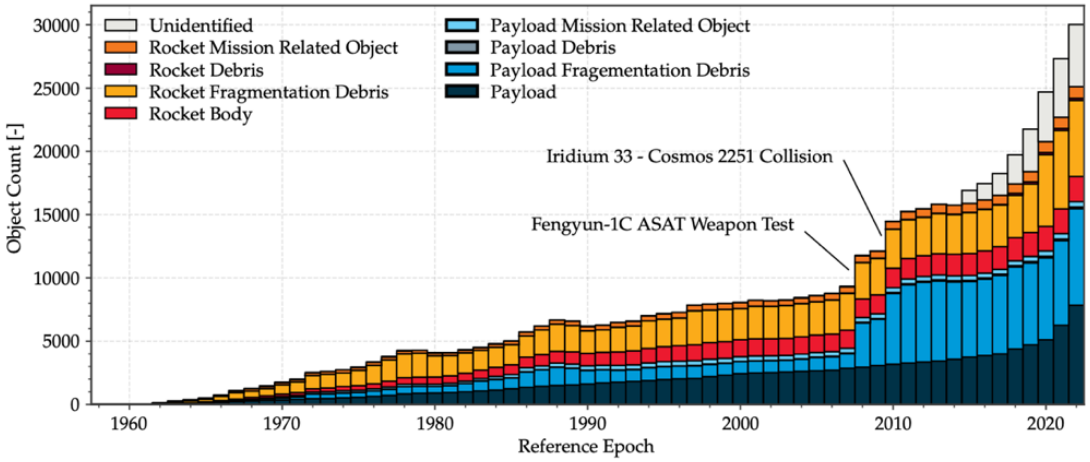

Fig. 1. *Time evolution of total object count in Earth orbit by type until 2022, adapted from [2].*

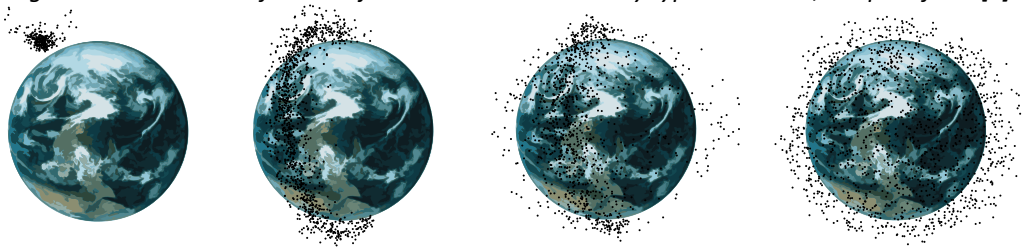

15 minutes 10 days 6 Months 3 years

Fig. 2. *Spreading of debris fragments from one initial position over time adapted from [8].*

To delay or prevent the rapid onset of the Kessler syndrome, many space debris removal methods have been proposed and investigated [10], ranging from capture methods for large debris objects [11–18] over passive methods to accelerate natural decay [19–24] to propulsion-based approaches [25–33], including applicability to small-size debris. Most of the literature focuses on the removal of large debris objects and prevention of break-up events, with less attention towards handling the consequence of such events. However, they result in a majority of debris with sizes between 1 and 10 cm, which are particularly important to remove from orbit [7].

For small-size debris, de-orbit through remote laser ablation propulsion is one of the most promising concepts, as it allows the application of thrust on objects remotely without reaction force on the removal spacecraft [34]. Laser ablation of a debris object permits to generate a thrust force as a reaction to a jet of gas and plasma created by ablating the surface layers of material with a strong incident laser beam. This presents the opportunity for extending the number of objects that can be targeted within one mission duration. While space-based laser ablation methods have previously been proposed for debris removal purposes and individual systems were analysed, a comprehensive feasibility analysis of a full mission to remove a large population of small debris has not yet been presented [28–32].

This work analyses the feasibility of active small debris removal through a space-based laser aiming to de-orbit 50% of 1 - 10 cm debris generated by a breakup event similar in magnitude to the 2009 Iridium-Cosmos collision, with a pre-breakup orbit below 1000 km altitude. The removal mission is assumed to be launched shortly after the breakup event to clean up the most hazardous debris. First, the mission concept performance is considered through a numerical model based on detection and ablation payload performance parameters. Then, key challenges of the supporting spacecraft design are considered and addressed. After presenting analysis on the technical feasibility, a mission cost estimate associated realising a laser-based debris removal mission are discussed and contextualised.

II. Mission Concept Feasibility

This section presents a performance analysis of the mission concept. First, the principles of laser ablation propulsion are described and an expression for the ΔV imparted is presented. Second, the Cosmos-Iridium debris dataset used as a reference case is reviewed. Third, the mission-level performance model is described in detail. Fourth, the results of the model are discussed, and the mission feasibility is shown to be a function of the payload performance. The simulation code has been made available under an open-source license and is available at https://github.com/eliasboegel/LDR.

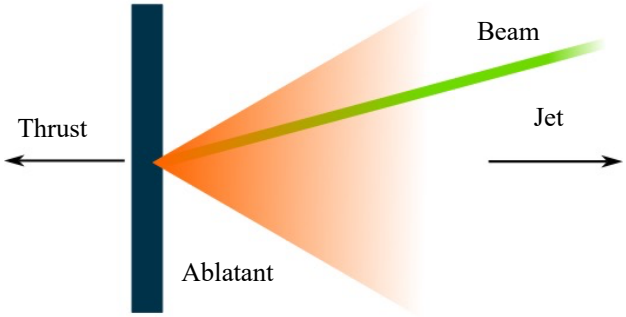

Fig. 3. *Thrust generation mechanism in laser ablation propulsion.*

A. Laser Ablation Propulsion Principles

A powerful pulsed or continuous wave laser beam can ablate a material into a jet of gas which may be partially ionised. This jet is ejected away from the surface, generating a thrust in the ablatant surface normal direction, as shown in Fig. 3 [35]. This principle can be leveraged to de-orbit small space debris in LEO.

Details on the physics of laser ablation propulsion can be found in [36, 37]. In this work, a pulsed diode-pumped Yb laser at 532 nm wavelength in the second harmonic is considered to evaluate the mission performance. The momentum imparted on an object is related to the energy received through the coupling coefficient C_m [29],

$$m\Delta v = C_m E \tag{1}$$

where m, Δv and E represent the mass of the object being ablated, the change in velocity opposite of the jet direction and the received energy, respectively. The energy received by an object is further dependent on the fluence ϕ, as $C_m = C_m(\phi)$ [29],

$$\phi = 4E_p T_{\text{eff}} \left(\frac{D_{\text{eff}}^2}{M^2 a_l^2 \lambda^2 L^2}\right)^2 \tag{2}$$

where E_p is the energy delivered in a single laser pulse, T_{eff} is the total system loss factor, D_{eff} is the effective diameter of the aperture, M^2 is the beam parameter product, a_l is a constant related to diffraction, λ is the wavelength and L is the distance between the laser and target at which the fluence ϕ is achieved. Assuming a common 6th order hypergaussian radial beam profile, $M^2 = 2$ and $a_l = 1.7$ [38]. There exists an optimum fluence ϕ_{opt} at which C_m, and hence the imparted momentum, is maximised for a given material and input energy. When the optimum fluence is significantly exceeded, the generated gas and plasma absorbs much of the incoming beam energy, shielding the ablatant surface. Phipps [29] proposes an empirical relation between ϕ_{opt} and the laser pulse duration τ with a constant B, which can also be related to the beam intensity at optimum fluence I_{opt},

$$\phi_{\text{opt}} \approx B\sqrt{\tau} = I_{opt}\tau. \tag{3}$$

Experimental data shows that a short pulse duration is desirable, but pulse lengths shorter than $\tau = 100$ ps show no additional advantages, therefore this value is used in this work [29]. Additionally, $B = 0.85$ GW/m^{2}s$^{0.5}$ shows good agreement across all materials [29], leading to $\phi_{\text{opt}} = 8.5$ kJ/m^2. Expressing the coupling coefficient as, $C_m = C_{m_0}/\left(I\lambda\sqrt{\tau}\right)^{0.25}$ and using $B = I_{opt}\sqrt{\tau}$ permits to write (4) for the optimum coupling coefficient [29],

$$C_{m,opt} = \frac{C_{m_0}}{(B\lambda)^{0.25}} \tag{4}$$

where C_{m_0} is a material-dependent constant. As a large portion of space debris consists of aluminium [39], the value of $C_{m_0} = 420$ N/MW for aluminium materials is used, yielding $C_{m,opt} = 91.1$ N/MW. The change in velocity of an object can then be expressed by rewriting $E_{opt} = \phi_{\text{opt}} A f t_{\text{abl}}$ in (1) with the object cross sectional area A, the pulse frequency f and total time targeted by the pulsed laser t_{abl}. This results in (5) which shows a dependence on the Area-to-Mass ratio (AMR) as the only object property.

$$\Delta v_{opt} = C_{m,opt}\phi_{opt}\left(\frac{A}{m}\right)_{\text{object}} f t_{\text{abl}} \tag{5}$$

B. Reference Fragment Population

The validated implementation of the NASA Standard Satellite Breakup Model (SSBM) from [40] is used to generate a reference dataset of debris originating from the 2009 Cosmos-Iridium collision. In this work, the 23091 satellite fragments with sizes between 1 and 10 cm from the Cosmos 2251 satellite are used to evaluate the mission performance. The SSBM then outputs the mass, area, and ejection velocity of each fragment based on statistical distributions and the initial velocities, masses and sizes of the colliding satellites [41]. The debris characteristics distributions are shown in Fig. 4.

The initial fragments position is given by the collision position in a circular orbit at an altitude of 789 km [42]. The initial fragments velocity is obtained by superimposing the pre-breakup satellite velocity and the ejection velocity computed from the SSBM for the considered particle. Furthermore, all debris are assumed to be inertially non-rotating spheres.

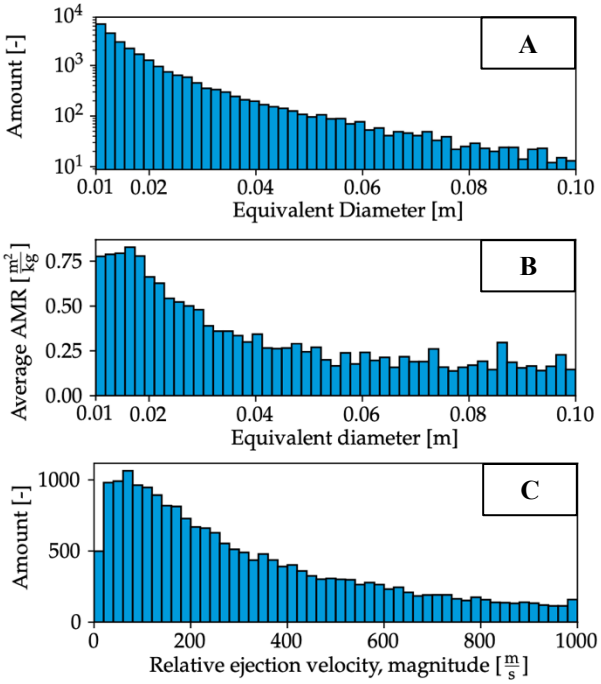

Fig. 4. Fragment number distribution (A), equivalent diameter (B), and relative ejection velocity magnitude (C) distributions of the reference dataset.

C. Mission Performance Model

To estimate overall mission performance, an agent-based model is devised. All debris fragments of the dataset are represented as inactive agents that are moved along their orbit but possess no ability to take actions. The spacecraft is also represented as an agent but has the capability to observe its surroundings within a fixed field of view (FOV) and can target debris using its laser system. The J_2 effect is considered, but atmospheric drag is neglected to reduce the computational load, resulting in a conservative estimate of the mission performance.

As the spacecraft cannot be launched immediately after the breakup event, but only after a certain time T_0, for $0 < t < T_0$, the spacecraft remains uninitialized while fragments are propagated along their orbits. At T_0, the spacecraft is initialised to the average fragment orbit with slightly increased altitude to minimise the angle to each fragment's velocity vector. The initial spacecraft inclination it set to the inclination of the pre-collision object related to the fragments to be removed.

All agents are propagated along their orbits in discrete time steps. To avoid the accumulation of numerical integration errors in the integration of the linearised equations of motion, the agent positions are represented by Keplerian elements: mean anomaly M, semi-major axis a, eccentricity e, inclination i, RAAN Ω and argument of pericentre ω. The orbit is propagated by integrating the mean anomaly in time t. As the mean anomaly is linear in time for unperturbed orbits, it can be integrated exactly. Additionally, the true anomaly θ is used as an input in the orbit propagation and can be computed by solving $M = \theta - e \sin\theta$ [7].

The behaviour of the spacecraft agent can be divided into two states: scanning and removal. During the scanning state, the spacecraft continuously points a lidar in the direction opposite of its velocity vector. While scanning, the spacecraft observes the space around its pointing direction with given circular FOV capped by the maximum detection range. When a debris object enters the capped cone of vision, the spacecraft detects the object with a delay equal to the scanning pattern time t_{scan}. Once a fragment is detected, the spacecraft estimates the time available for ablation of the fragment, which is limited by the trajectory of the fragment and the spacecraft, as well as the angle between the fragment velocity vector and the relative position vector from fragment to spacecraft and is estimated using the bisection algorithm with a fixed large time step $\Delta t = t_{\text{min}} = t_{\text{scan}} + t_{\text{abl}}$.

Consider the visibility function v for a given fragment taking the value 0 or 1 if the fragment is outside or inside the cone of vision respectively. $v(t)$ may be evaluated at any discrete point in time t_i by propagating the Kepler state of both the spacecraft and the fragment to time t_i and evaluating the visibility conditions at this time. With this, it is possible to formulate an efficient method to determine the visibility time t_{vis} for a given intersection of a fragment while retaining a large time step to skip over periods without fragments in the cone of vision. An illustration of the method is outlined in Fig. 5: a) the interval can only miss all sample points if $t_{\text{vis}} < t_{\text{min}}$, meaning the fragment is always correctly skipped; b) t_{vis} is evaluated using bisection and the fragment is targeted if $t_{\text{vis}} > t_{\text{min}}$; c) the fragment is targeted as $t_{\text{vis}} > t_{\text{min}}$ holds.

If $t_{vis} > t_{\text{min}}$ the spacecraft switches to its removal state and the ablation laser shoots at the debris fragment. The system aims to decrease the pericentre altitude of ablated fragments below 340 km, as natural decay simulations (using the NRLMSISE-00 model at a worst-case low solar cycle [43]) for a fragment with the minimum AMR contained in the dataset can de-orbit naturally from an elliptical orbit with 1000 km apocenter altitude and 340 km pericentre altitude within one year. Therefore, a debris object is considered removed once its pericentre altitude has been lowered to below 340 km. The simulation is stopped once the stopping criteria given by (6) is fulfilled,

$$0.5 \leq \frac{\#\ debris\ removed}{\#\ total\ debris}. \qquad (6)$$

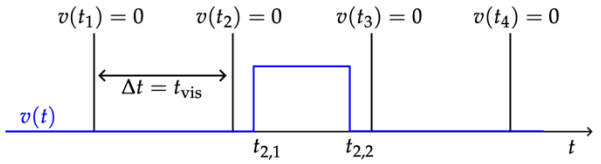

a) Fragment visible for an interval that falls between intersection point.

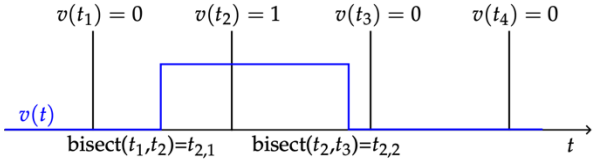

b) *Fragment visible for an interval meeting one sampling point.*

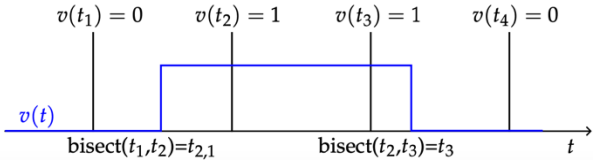

c) *Fragment visible for an interval long enough to cover multiple sampling points.*

Fig*. 5. Time stepping and fragment-spacecraft intersection.*

The Gauss perturbation equations from [7] are used to express the change in Keplerian elements resulting from $\boldsymbol{\Delta V}$. These equations take the input ΔV in the RTN frame, a spacecraft-centred coordinate system where R is parallel to the position vector, N is perpendicular to the orbital plane, and T completes the right-handed coordinate system. Furthermore, as no information is available on the shape and the rotational state of the fragment, it is assumed that the thrust occurs in the direction opposite to the velocity vector. This assumption is based on the orbit chosen for the active agent, which favours head-on geometries. Therefore, the out-of-plane component can be assumed zero, as the vector opposite of the fragment velocity is always in-plane. This results in the following modified discrete Gauss perturbation equations,

$$\Delta a = \sqrt{\frac{a}{\mu}}\frac{2a}{\sqrt{1-e^2}}(\sin\theta\,\Delta V_r e + (1+e\cos\theta)\Delta V_t) \quad (7)$$

$$\Delta e = \sqrt{\frac{a}{\mu}}\sqrt{1-e^2}\left[\sin\theta\,\Delta V_r + \frac{e+2\cos\theta+e\cos^2\theta}{1+e\cos\theta}\Delta V_t\right] \quad (8)$$

$$\Delta\omega = \sqrt{\frac{a}{\mu}}\frac{\sqrt{1-e^2}}{e}\left[-\cos\theta\,\Delta V_r + \frac{2+e\cos\theta}{1+e\cos\theta}\sin\theta\,\Delta V_t\right] \quad (9)$$

$$\Delta M = n + \frac{1-e^2}{nae}\left[\left[\cos\theta - \frac{2e}{1+e\cos\theta}\right]\Delta V_r - \frac{2+e\cos\theta}{1+e\cos\theta}\sin\theta\,\Delta V_t\right] \quad (10)$$

where μ is Earth's gravitational parameter and $n = \sqrt{\mu/a^3}$ is the mean motion. These equations are accurate only for small values of ΔV_r and ΔV_t, hence the total $\boldsymbol{\Delta V}$ to be applied is partitioned into small velocity changes of up to 0.01 m/s in magnitude, which are applied in sequence to keep integration errors to a minimum. Furthermore, once a debris has been targeted, the heat generated by the ablation laser system needs to be radiated away, yielding a cooldown time t_{cd}.

The J_2 orbit correction is similarly applied at every propagation time step using (11-13) [7]. However, as these equations are also only valid for small Δt, the time step shall be chosen small enough.

$$\Delta\Omega = -\frac{3}{2}nJ_2\left[\frac{R_e}{a(1-e^2)}\right]^2\cos(i)\Delta t \quad (11)$$

$$\Delta\omega = \frac{3}{4}nJ_2\left[\frac{R_e}{a(1-e^2)}\right]^2(4-5\sin^2 i)\Delta t \quad (12)$$

$$\Delta M = n\left[1+\frac{3}{4}J_2\left[\frac{R_e}{a(1-e^2)}\right]^2(2-3\sin^2 i)\sqrt{1-e^2}\right]\Delta t \quad (13)$$

Throughout the simulation, the number of fragments marked as removed is recorded over time. The model is implemented using the Julia language and fragment position updates are fully parallelized over all available CPU cores. In total, over 2300 mission configurations were analysed. Due to the total workload involved, all configurations were analysed using CPU compute nodes of the DelftBlue Phase 1 system of the Delft High Performance Computing Centre (DHPC) [44].

D. Simulation Results

A variety of spacecraft parameters were varied to evaluate the feasibility of the mission concept. As a baseline, a spacecraft with $r_{abl} = 250$ km, $t_{scan} = 5$ s, $t_{abl} = 50$ s (and consequently $t_{min} = 55$ s) at FOV= 37.91° is used with a cooldown time between payload uses of $t_{cd} = 70$ s. The maximum incidence angle between the incoming beam direction and the velocity vector of a fragment is set to 20°. The spacecraft is placed in a circular orbit 30 km above the original collision altitude. The scan range is always 50 km more than the ablation range. Unless otherwise specified, the baseline case parameters are used for analysis below except for the parameters being varied for analysis.

First, the ablation laser maximum range was varied between 200 km and 300 km, whereas the ablation time was varied between 20 and 90 seconds. The effect of launch delay on the mission performance is also investigated. Fig. 6 shows the relation between the varied payload parameters for a 50% removal time of one year (all combinations above the line result in mission success within a year). The envelope is limited by a border with steep increase in mission time, which can be decomposed into two lines that constrain the mission feasibility: a line limiting the short and long ablation time ends of the envelope. The long ablation time limit represents the increase of the minimum visibility time of a fragment encounter beyond the time

a fragment encounter typically lasts. On the other hand, the short ablation time limit represents the decrease of imparted energy per ablation laser shot to levels so low that targeted fragments no longer change orbit enough for their new orbit to decay naturally. Furthermore, the achievable launch delay drives up ablation and detection laser payload requirements. After 15 days of launch delay, the natural spread of the debris cloud result in fragment encounters becoming rare enough to make the mission impossible for certain detection and ablation ranges. For the Cosmos-Iridium event, the same mission performance is obtained with a launch delay of 1 day using an ablation range of 220 km, as with an ablation range of 260 km after a 15 days delay.

Secondly, two main parameters of the detection payload are varied and the effects on mission performance are recorded. For the lidar-based object detection system, at 250 km detection range and an average power 250 W, Fig. 7 shows a base FOV of ≈ 0.1711°. This base was set by comparing the expected incoming signal strength to the cosmic background radiation and ensuring a Signal-to-Noise ratio of 2. To increase the effective FOV, a scanning pattern is employed at the cost of a longer scanning time, resulting from the lidar imaging frequency, since the images require a certain overlap to avoid gaps in the scanning field. To quantify this effect on the mission performance and evaluate feasibility as a function of the detection payload performance, the 50% removal time is determined for variations in both parameters. Following Fig. 8, the feasibility envelope is limited by both the low and the high scanning times (low and high FOV respectively). On the low scanning time boundary, this can be explained by the very low FOV and narrow detection cones, which shorten the visibility time for a passing fragment. For the high scanning time, the boundary appears as the scanning time required grows to an extent where the visibility time of a passing fragment becomes too short even with the accordingly increased FOV. Furthermore, greater ranges provide a larger design space to use longer scan times in exchange for larger FOV values. All ranges show feasible operation around a scan time of 10 s, providing a sufficiently short visibility time requirement and a large enough FOV for the system to be efficient.

III. Spacecraft Design Feasibility

A. Overall Design

The spacecraft detects space debris based on a lidar system and ablates them using a Nd:YAG laser operating at 532 nm. Operations of the laser for debris removal activities result in a peak power of 27.7 kW over a period of 50 s. The total spacecraft mass is 2794 kg (350 kg of propellant mass for orbit maintenance) and can be launched using an Ariane 62 with its short fairing. An overview of the complete spacecraft structure is show in Fig. 9, which was selected to fit the launcher centre of mass requirements despite the heavy lidar system mounted on the top of the spacecraft. It is noted that the gimbal system is the most uncertain subsystem of the spacecraft and is assumed to take up the entire compartment shown in Fig. 9 with a load-carrying structure. Furthermore, the heat pipes are distributed over the Power Conditioning and Distribution Unit (PCDU), batteries, and laser assembly surface, and they are connected to the inner surface area of the radiators.

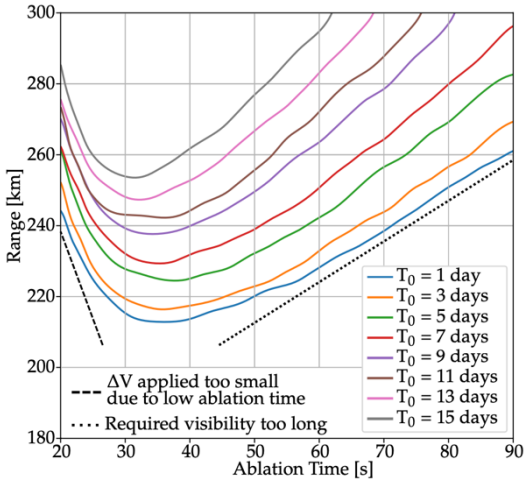

Fig. *6. Feasibility envelope on payload parameters ablation range and ablation time as a function of launch delay. Combinations above the line result in removal times within 1 year.*

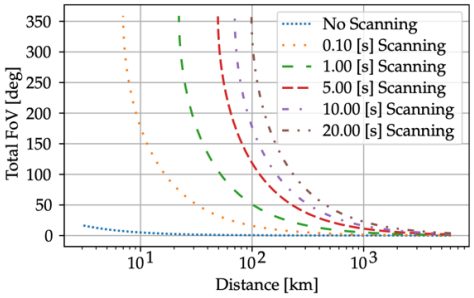

Fig. *7. Relation between the FOV as a function of maximum detection range and scanning time.*

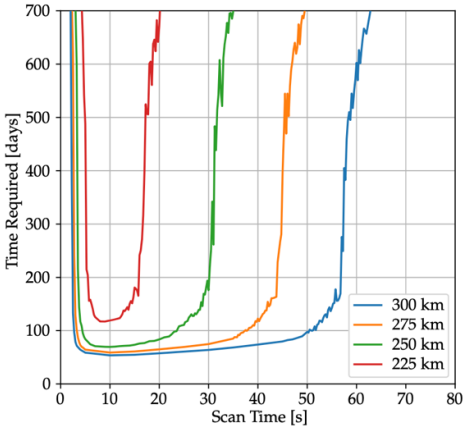

Fig. *8. 50% removal time as a function of the scanning time for different ablation ranges.*

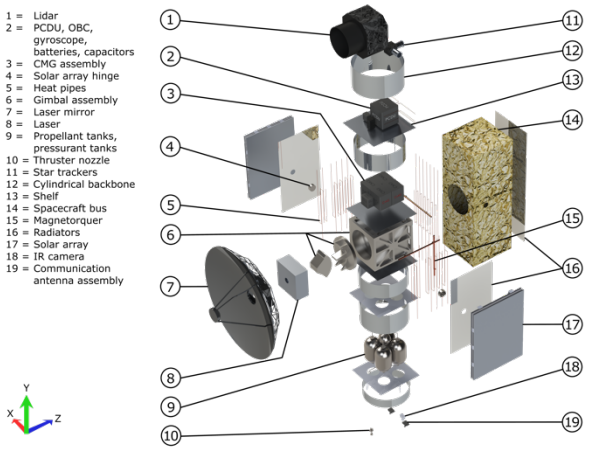

Fig. 9. Exploded view of the spacecraft design.

Table 1. Subsystem power overview.

Subsystem	Power [W]	Subsystem	Power [W]
Payload	5300	CDHS	25.64
TT&C	3.1	TMS	23.5
EPS	100	Structures	500
GNC	880	Propulsion	72

B. Debris Detection and Removal Payload

Most likely relying on two mirrors working together, the laser must be reflected off a secondary (smaller) mirror onto a primary (larger) mirror to generate the spot size required for a given range. As fluence is a function of the laser mirror diameter, and an optimum fluence of 8.5 kJ/m^2 was selected [29], the mirror was determined to be 4.02 m in diameter to allow for optimal fluence for a spot size of 0.125 m up to a range of 250 km. The mass of the mirror system is estimated at 581 kg.

The laser itself is an Nd:YAG laser operating at 532 nm, the second harmonic. The pulse geometry is defined by a pulse duration of 100 ps, a repetition rate of 55.8 Hz and a pulse energy of 116 J. These parameters result in a laser mass of 564 kg, bringing the total ablative payload mass to 1150 kg. However, both the laser and mirror systems will require extensive further Research and Development before reaching the required Technology Readiness Level (TRL). These include theoretical studies on the performance of laser ablation on different materials and rotational regimes, and optimisation of the mirror structure.

The Nd:YAG 532 nm lidar system operates at an average power of 243 W (10 MW pulse power), for a mass of 286 kg. Each 1 ns pulse has an energy of 10 mJ, and with a repetition rate of 10 kHz and 200x200 pixels sensor, a spatial resolution of 5 mm at 300 km detection range with a distance resolution of 12 cm. Moving optics technology needs to be developed to adapt the FOV right before and during ablation, and the transmitter must vary the duration, shape, phase, or interval of each pulse to distinguish one received signal from another.

C. Electrical Power Subsystem

The complete system has 6.9 kW of average power and the 27 kW of peak power during the mission, with the breakdown shown Tab. 1 (where TT&C refers to the Telemetry, Tracking and Command subsystem and CDHS refers to the Command and Data Handling Subsystem). Therefore, the Electrical Power Subsystem (EPS) consists of a 35 m^2 solar array, a set of Li-Ion batteries, a PCDU, and a set of Li-Ion capacitors to power the laser. While batteries are used to power the spacecraft bus during eclipse times, capacitors are used to power the laser during the 50 s shooting window due to their faster discharge times. The use of a solar array also makes the design modular to missions with different orbits. In the most challenging scenario, the subsystem weighs up to 166 kg.

The system requirements are met by Commercial Off-The-Shelf Components (COTS) for all components except the PCDU, which needs to be designed for the mission specifically to sustain the 27 kW of power during the laser shooting periods. Another option is to use a COTS specifically for the spacecraft bus, and design one from the ground-up for the laser and capacitors. Additionally, the scale of the design is dependent on the maximum number of debris detected and ablated through a single orbit. This design is capable to generate enough power for a maximum of 243 particles per day, which was determined based on the mission analysis model.

D. Guidance Navigation and Control Subsystem

The system's target orbit of 30 km above the average debris orbit at launch was chosen by simulating the mission performance model using different relative altitudes. Namely, the selected altitudes ranged from 0 to 100 kilometres above the original collision orbit, with the simulation being run in steps of 10 km. Results proved that the selected target orbit was the one at which the system performed the best.

Using a simplified 2D model, the system was found to require an attitude determination and pointing accuracy of $4.52 \cdot 10^{-5}$ radians around all axes. Furthermore, the minimum disturbance torque that the system shall endure was found to be 0.012 Nm. As done with the electrical power subsystem, requirements were met by selecting a range of COTS star sensors and gyroscopes for attitude determination, and CMGs and magnetic torquers for attitude control. The final Guidance Navigation and Control (GNC) subsystem has a mass of 355.8 kg and a nominal power of 388 W.

E. Thermal Management Subsystem

With extreme power draw during ablation operations at only 25.2% efficiency, the Thermal Management Subsystem (TMS) must be able to transport away and reject approximately 26 kW of waste power during

active periods of the ablation laser. This requires a strong thermal connection from the primary payload, and connected subsystems like the battery and capacitor units, as well as the PCDU. This calls for heavy use of heat pipes and efficient radiators with Optical Solar Reflector (OSR) surfaces. 35 heat pipes of 8 mm diameter connect the laser system to 16 m^2 of radiators, with four further heat pipes connecting both the PCDU, and the Li-ion batteries to another 2.4 m^2 set of OSR radiators. As the average power consumption throughout the mission decreases drastically, variable conductance heat pipes are employed to control the amount of heat rejected. The TMS design chosen has a mass of 65 kg and requires 74 W.

F. Design Feasibility

The resulting bus design is fully feasible with current technology (except the PCDU). However, the laser ablation payload will require a significant amount of research and development to reach the required TRL and remains a large area of uncertainty. Development plans focus on performing experiments regarding debris characteristics (size, shape, material, rotational velocities), developments of the laser technology itself, and mirror developments for both the lidar and laser technologies.

IV. Economic Considerations

While it has now been shown that a large portion of a post breakup event orbit can be cleaned up with a laser ablation propulsion concept, it has not yet been established whether the corresponding mission and system is feasible economically. Workforce, logistics and associated (workspaces, insurances) costs were considered through per-employee cost estimates and assigned staff numbers of previous European Space Agency (ESA) projects of similar magnitude. Cost estimates of every subsystem of the conceptual design were obtained as part of the feasibility study. The cost distribution for each subsystem is determined based on market prices for similar systems. In the special case of the payload systems, additional costs for R&D of space-suitable laser and lidar systems are incorporated. Beyond the acquisition cost of each subsystem, costs associated with the verification, validation and testing processes for each system in the design are also included. Expressing the uncertainty in the cost of each component, an estimated single-system mission cost probability function was obtained in Fig. 10. The obtained most likely cost estimate of approximately 550 M€ agrees well with the cost estimate for the most similar configuration of the proposed L'ADROIT system, for which a cost of 560M$ [29] was suggested.

Furthermore, while the cost for a single system as estimated in Fig. 10 is high, the mission concept targeting specifically mitigation of breakup events

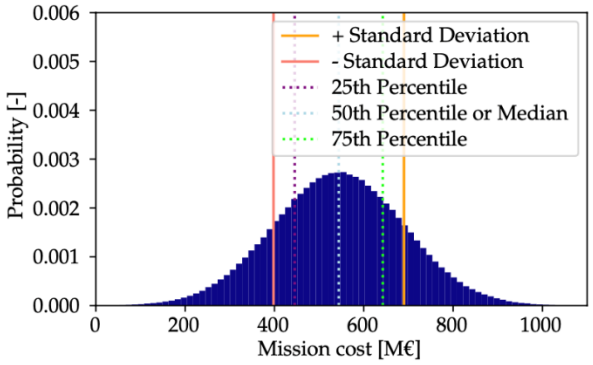

Fig. 10. Single-system mission cost estimation with uncertainties as a probability. The probability distribution is generated based on uncertainties in individual component and labour costs.

requires the system to be ready on short notice (on the order of days) once such an event has occurred. Therefore, the system is not developed and produced for each case individually, and costs associated with the design and development of the system must be treated as single-time costs when considering series production and deployment of the system. Design and development costs alone account for an estimated 58% of total costs (44% R&D and 14% design), with only 42% of the estimated mission cost applicable to any produced unit beyond the initial prototype (21% for the launch). Small series production may also lower the cost component associated with the production of the system.

While the cost of such mission is relatively high, it is a rather small investment compared to the potential loss of services in LEO. The value of the space market in LEO altitude bands in 2021 was estimated to be approximately 3.50 B$ and is expected to grow to 9.0 B$ by 2026 (FY2021 US$) [45].

V. Conclusion

This study showed the feasibility of a space-based laser mission for small space debris removal. The system was tested based on the Cosmos-Iridium collision, showing that it can deorbit 50% of the fragments within a year, and can be supported by a spacecraft bus with state-of-the-art components. The debris detection and removal payload, however, will still require extensive R&D. The mission is also economically feasible, with a most likely cost estimate of 550M€ (FY2022) for a single mission, which can be lowered through small series production.

VI. Acknowledgements

The authors thank Prof. Erwin Mooij, Prof. Nathan Eskue and Dr. Iklim Akay of the *TU Delft Aerospace Engineering Faculty*, as well as Dr. Claude Phipps of *Photonic Associates LLC* and Dr. Fabio di Teodoro of *Raytheon Space and Airborne Systems* for their detailed advice and support.

VII. REFERENCES

[1] A.K. Maini and V. Agrawal. *Satellite technology: principles and applications*. John Wiley & Sons, 2011.

[2] European Space Agency Space Debris Office. *"ESA'S Annual Space Environment Report"*. No. GEN-DB-LOG-00288-OPS-SD, European Space Agency, 2023.

[3] D.J. Kessler and B.G. Cour-Palais. "Collision frequency of artificial satellites: The creation of a debris belt," *Journal of Geophysical Research: Space* Physics, vol. 83, no. A6, pp. 2637-2646, 1978.

[4] A.C. Boley and M. Byers. "Satellite mega-constellations create risks in Low Earth Orbit, the atmosphere and on Earth," *Scientific Reports*, vol. 11, no. 1, pp. 1-8, 2021.

[5] P. Anz-Meador, John Opiela, and Jer-Chyi Liou. *History of on-orbit satellite fragmentations*. No. NASA/TP-20220019160, 2023.

[6] J. Sankaran, "Russia's anti-satellite weapons: A hedging and offsetting strategy to deter western aerospace forces," *Contemporary Security Policy*, vol. 43, no. 3, pp. 436 – 463, 2022.

[7] H. Klinkrad. *Space debris: models and risk analysis*. Springer Science & Business Media, 2006.

[8] D. Wright, "Space debris," *Physics Today*, vol. 60, no. 10, pp. 35 – 40, 2007.

[9] D. Casanova, A. Petit, and A. Lemaître, "Long-term evolution of space debris under the J2 effect, the solar radiation pressure and the solar and lunar perturbations," *Celestial Mechanics and Dynamical Astronomy*, vol. 123, no. 2, pp. 223 – 238, 2015.

[10] P. Y. Zhao, J. G. Liu, and C. C. Wu, "Survey on research and development of on-orbit active debris removal methods," *Science China Technological* Sciences, vol. 63, no. 11, pp. 2188 – 2210, 2020.

[11] Z. Mu and W. Xu and B. Liang, "Avoidance of multiple moving obstacles during active debris removal using a redundant space manipulator," *International Journal of Control, Automation and Systems*, vol. 15, no. 2, pp. 815 – 826, 2017.

[12] X. Zhang and J. Liu, "Effective motion planning strategy for space robot capturing targets under consideration of the berth position," *Acta Astronautica*, vol. 148, pp. 403 – 416, 2018.

[13] J. Choi, J. Jung, D. Lee, and B. Kim, "Articulated linkage arms based reliable capture device for janitor satellites," *Acta* Astronautica, vol. 163, no. 3, pp. 91 – 99, 2019.

[14] X. Li, K. Sun, and H. Liu, "Design of a novel deployable mechanism for capturing tumbling debris," *Transactions of the Canadian Society for Mechanical Engineering*, vol. 43, no. 3, pp. 294 – 305, 2019.

[15] Y. Zheng, G. Lei, M. Zhang, and Q. Che, "Mechanical design and analysis of a gripper for non-cooperative target capture in space," *Advances in Mechanical Engineering*, vol. 10, no. 11, 2018.

[16] C. Sun, W. Wan, and L. Deng, "Adaptive space debris capture approach based on origami principle," *International Journal of Advanced Robotic* Systems, vol. 16, no. 6, 2019.

[17] H. Jiang, E. W. Hawkes, C. Fuller, M. A. Estrada, S. A. Suresh, N. Abcouwer, A. K. Han, S. Wang, C. J. Ploch, A. Parness, and M. R. Cutkosky, "A robotic device using gecko-inspired adhesives can grasp and manipulate large objects in microgravity," *Science Robotics*, vol. 2, no. 7, pp. eaan4545, 2017.

[18] M. Shan, J. Guo, and E. Gill, "An analysis of the flexibility modeling of a net for space debris removal," *Advances in Space* Research, vol. 65, no. 3, pp. 1083 – 1094, 2020.

[19] M. Andrenucci, P. Pergola, R. A., J. Olympio, and L. Summerer, "Expanding foam application for active debris removal," ESA Advanced Concepts Team, pp. 10- 6411, 2011.

[20] N. Takeichi, "Practical operation strategy for deorbit of an electrodynamic tethered system," *Journal of Spacecraft and Rockets*, vol. 43, no. 6, pp. 1283 – 1288, 2006.

[21] Y. Ishige, S. Kawamoto, and S. Kibe, "Study on electrodynamic tether system for space debris removal," *Acta* Astronautica, vol. 55, no. 11, pp. 917 – 929, 2004.

[22] E. J. van der Heide and M. Kruijff, "Tethers and debris mitigation," *Acta Astronautica*, vol. 48, no. 5, pp. 503 – 516, 2001.

[23] L. Tarabini Castellani, S. García González, A. Ortega, S. Madrid, E. Lorenzini, L. Olivieri, G. Sarego, A. Brunello, A. Valmorbida, M. Tajmar, C. Drobny, J.-P. Wulfkuehler, R. Nerger, K. Wätzig, S. Shahsavani, and G. Sánchez-Arriaga, "Deorbit kit demonstration mission," *Journal of Space Safety Engineering*, vol. 9, no. 2, pp. 165 – 173, 2022.

[24] G. Feng, W. Li, and H. Zhang, "Geomagnetic energy approach to space debris deorbiting in a low earth orbit," *International Journal of Aerospace Engineering 2019*, 2019.

[25] V. Balashov, M. Cherkasova, K. Kruglov, A. Kudriavtsev, P. Masherov, A. Mogulkin, V. Obukhov, V. Riaby, and V. Svotina, "Radio frequency source of a weakly expanding wedge-shaped xenon ion beam for contactless removal of large-sized space debris objects," *Review of Scientific Instruments*, vol. 88, no. 8, 2017.

[26] K. Takahashi, C. Charles, R. W. Boswell, and A. Ando, "Demonstrating a new technology for space debris removal using a bi-directional plasma thruster," *Scientific Reports*, vol. 8, no. 1, 2018.

[27] F. Cichocki, M. Merino and E. Ahedo, "Spacecraft-plasma-debris interaction in an ion beam shepherd mission," *Acta Astronautica*, vol. 146, pp. 216 – 227, 2018.

[28] S. Scharring, J. Wilken, and H-A. Eckel, "Laser-based removal of irregularly shaped space debris," *Optical Engineering*, vol. 56, no. 1, 2016.
[29] C. R. Phipps, "L'Adroit - a spaceborne ultraviolet laser system for space debris clearing," *Acta Astronautica*, vol. 104, no. 1, pp. 243 – 255, 2014.
[30] S. H. Choi and R. S. Pappa, "Assessment study of small space debris removal by laser satellites," in *IEEE Aerospace Conference*, NASA Langley Research Center, 2011.
[31] R. Battiston, W. Burger, A. Cafagna, C. Manea, and B. Spataro, "A systematic study of laser ablation for space debris mitigation," *Journal of Space Safety Engineering*, vol. 4, no. 1 , pp. 36 – 44, 2017.
[32] L. Peeters and R. Noomen, "Active small-scale space debris removal by a space-based laser," Master's thesis, Delft University of Technology, 2020.
[33] C. R. Phipps and J. P. Reilly, "ORION: clearing near-Earth space debris in two years using a 30-kW repetitively-pulsed laser," in *11th International Symposium on Gas Flow and Chemical Lasers and High- Power Laser Conference*, vol. 3092 D. R. Hall and H. J. Baker, eds., International Society for Optics and Photonics, pp. 728 – 731, SPIE, 1997.
[34] L. Pieters and R. Noomen, "Simulating arbitrary interactions between small-scale space debris and a space-based pulsed laser system," *Advances in Space Research*, vol. 72, no. 7, pp. 2778–2785, 2023.
[35] C. R. Phipps, M. Birkan, W. Bohn, H.-A. Eckel, H. Horisawa, T. Lippert, M. Michaelis, Y. Rezunkov, A. Sasoh, W. Schall, S. Scharring, and J. Sinko, "Review: Laser-ablation propulsion," *Journal of Propulsion and Power*, vol. 26, no. 4, pp. 609 – 637, 2010.
[36] C. R. Phipps, K. L. Baker, S. B. Libby, D. A. Liedahl, S. S. Olivier, L. D. Pleasance, A. Rubenchik, J. E. Trebes, E. Victor George, B. Marcovici, J. P. Reilly, and M. T. Valley, "Removing orbital debris with lasers," Advances in Space Research, vol. 49, no. 9, 1283 – 1300, 2012.
[37] C. R. Phipps, *Laser Ablation Propulsion and Its Applications in Space*, Springer International Publishing, Cham, 2018.
[38] C. R. Phipps, D. E. Watkins, and S. J. Thomas, "Effect of nonlinear refraction on beam brightness in laser fusion applications," in *International Conference on Lasers*, Los Alamos National Laboratory, 1979.
[39] J. N. Opiela, "A study of the material density distribution of space debris," *Advances in Space Research*, vol. 43, no. 7, pp. 1058 – 1064 (2009).
[40] J. Schuhmacher, "Efficient Implementation and Evaluation of the NASA Breakup Model in modern C++," Bachelor's thesis, Technical University of Munich, 2021.
[41] N.L. Johnson, P.H. Krisko, J-C. Liou and P.D. Anz-Meador, "NASA's new breakup model of Evolve 4.0," *Advances in Space Research*, vol. 28, no. 9, pp. 1377–1384, 2001.
[42] A. Tan, T. X. Zhang and M. Dokhanian, "Analysis of the Iridium 33 and Cosmos 2251 Collision using Velocity Perturbations of the Fragments," *Advances in Aerospace Science and Applications,* vol. 3, no. 1, pp. 13–15, 2013.
[43] J.M. Picone, A.E. Hedin, D.P. Drob and A.C. Aikin, "NRLMSISE-00 empirical model of the atmosphere: Statistical comparisons and scientific issues", *Journal of Geophysical Research: Space Physics*, vol. 107, no. A12, 2002.
[44] Delft High Performance Computing Centre (DHPC), "DelftBlue Supercomputer (Phase 1)," https://www.tudelft.nl/dhpc/ark/delftbluephase1, 2022.
[45] The Business Research Company, "Low Earth Orbit (LEO) Satellites Global Market Report 2022," Technical report, 2022.